Wear behavior of carbide coated Co–Cr–Mo implant alloy

N. S. VANDAMME, B. H. WAYMAN, L. D. T. TOPOLESKI
Department of Mechanical Engineering, UMBC, Baltimore, MD 21250, USA

The wear behavior of a new type of metal carbide surface coating on Co–Cr–Mo implant alloy was studied. The coating was created using a microwave plasma-assisted reaction. Codeposition of impurity diamond film, diamond particles, and soot was prevented by controlling process conditions. Wear tests were carried out using a sapphire ball-on-Co–Cr–Mo disc unidirectional sliding configuration with harsh conditions of high contact stress and slow sliding speed in both no-lubrication, and deionized water lubrication environments. In the case of uncoated Co–Cr–Mo discs, the effect of deionized water lubrication was remarkable and reduced the wear factor by one order of magnitude compared to the no-lubrication tests. The wear factor of carbide coated Co–Cr–Mo discs was slightly smaller than that of uncoated Co–Cr–Mo discs with deionized water lubrication ($2.7 \times 10^{-6}\,mm^3\,N^{-1}m^{-1}$ *vs.* $4.2 \times 10^{-6}\,mm^3\,N^{-1}m^{-1}$). The addition of deionized water lubrication did not greatly affect the wear factor of carbide coated Co–Cr–Mo discs. The influence of surface geometry resulting from the ''brain coral-like'' surface morphology of carbide layers on wear behavior was analyzed considering stress concentrations and effective contact area.

1. Introduction

The use of artificial joints is increasing rapidly and such implants are required to have a longer service life. There is growing concern about the wear of materials used in artificial joints. Since the production of excessive amounts of polyethylene wear debris has been linked to osteolysis, which may result in further component loosening, a low wear rate for implants is believed to be critical for extending the implant service time [1, 2]. The concept of metal-on-metal implants has been renewed for total hip replacements and various aspects of metal-on-metal bearings have been studied [3–10]. Furthermore, as excellent wear resistant materials, ceramics have been investigated in combination with ultra-high molecular weight polyethylene, alloys, and ceramics [11–17].

Surface modification is one important approach to improving wear resistance. For example, amorphous diamond-like carbon coatings [18–22] and ion implantation [23–26] have been studied to improve the wear resistance of implant materials.

The formation of metal carbide surface layers on a Co–Cr–Mo alloy by the reaction between the alloy surface and gases by a microwave plasma-assisted surface reaction was reported by the present authors [27]. This newly developed carbide coated Co–Cr–Mo showed a potential to improve the wear performance of Co–Cr–Mo alloy joints because carbide-coated Co–Cr–Mo has a unique ''brain coral-like'' surface morphology and a wide range of hardness from HV 1000 to HV 2100, and is a functionally graded material composed of a ceramic carbide surface layer, carbon diffused subsurface layer, and original alloy matrix [27].

In this study, the wear properties of carbide coated Co–Cr–Mo have been investigated in harsh wear conditions with sapphire ball-on-disk unidirectional sliding tests and compared to an uncoated Co–Cr–Mo implant alloy.

2. Materials and methods

A wrought Co–Cr–Mo alloy rod (ASTM F1537, Teledyne Allvac) of 0.625 inch in diameter was cut into 7-mm thick discs. The manufacturer's specifications gave the primary composition of the alloy as 64.85-wt % Co, 27.66-wt % Cr, and 5.70-wt % Mo. The carbon content of the alloy was 0.048-wt %. Prior to plasma processing, the top and bottom flat surfaces of the discs were polished to a ''mirror finish'' with #600 and #1000 SiC abrasive paper, then with a 3-μm diamond suspension, and ultrasonically cleaned with acetone. The average roughness (Ra) was $\sim 0.01\,\mu m$, measured with a white light interference surface profilometer (New View 100, Zygo Inc., CT). The cylindrical side surface and rounded edges were also polished similarly but had a rougher finish.

The microwave plasma-assisted reaction was carried out using our microwave plasma-assisted chemical vapor deposition system equipped with a tubular fused quartz reaction chamber with a 34 mm inner diameter. The microwave generator (Toshiba Corp., Tokyo) provides a range of microwave power from 0.1 to 1.5 kW at a frequency of 2.45 GHz. The Co–Cr–Mo specimens were

mounted on a tantalum wire basket holder and inserted into a confined plasma space on a fused quartz rod. Plasma processing was carried out in a mixture of methane (Ultra High Purity 99.97%) and hydrogen (Zerograde 99.99%) with a total gas pressure of 70 Torr and a total gas flow rate of 100 sccm (1 sccm of methane and 99 sccm of hydrogen) for 6 h. Before introducing methane, the specimens were immersed in hydrogen plasma for 15 min. The specimen temperature was controled by changing the microwave input power and set to 500 W ($\pm$ 20 W) for the specimen to be maintained at 990 $\pm$ 5 °C which was measured with an optical pyrometer (Leeds and Northrup Model 8622) through the quartz-glass viewport at the top of the reaction chamber.

The total thickness of the surface coatings was estimated from micrographs of a polished section of the side plane of the substrate taken using a scanning electron microscope (SEM) (JEOL JSM-35 CF). The coating thickness was also estimated by weight change measured using an analytic balance (Mettler AG 245) with an accuracy of 10 μg and the density of chromium carbide.

The surface morphology of carbide coated Co–Cr–Mo discs was studied with the profilometer. The roughness parameters including average roughness, mean peak-to-valley height, core roughness depth, reduced peak height, reduced valley depth, peak material ratio, valley material ratio, number of peaks or valleys, and peak or valley spacing [28] were obtained from the measurement of nine equally spaced locations along the diameter of each disk. The filter cutoff wavelength, which differentiates between roughness and waviness, was fixed at 20 μm after measuring the cutoff wavelength dependence of the average roughness and core roughness depth of three carbide coated specimens.

The wear properties of the specimens were studied using a unidirectional rotational ball-on-disk wear testing machine equipped with three specimen holders and three load and pin assemblies, which were mounted on the free ends of three 25-cm-cantilevers [29]. The disc's rotation was powered by a speed-controlled synchronous motor. Rotating speeds of the discs could be varied from 5 rpm to 40 rpm. Grade 25 sapphire balls of 3/32 inch diameter (Small Parts Inc., FL) were used as the counterbody against uncoated and carbide-coated Co–Cr–Mo discs to compare the wear behavior of discs without substantial wear of the counterbody. Ball-on-disk tests were carried out in a single station of the three station-testing machine to obtain identical measuring conditions for each specimen. The test conditions used in the present study were: a 4.8 N dead load, 17-mm s^{-1} sliding speed, no-lubrication at room temperature, and deionized water lubrication at 37 ($\pm$ 2) °C. Deionized water was maintained at a constant temperature in a reservoir and supplied continuously over the wear surface of the discs. A new specimen disc, coupled with a new sapphire ball, was used during every wear test period (1 h, 3 h, and 5 h). The wear volume was determined from the wear track cross-sectional areas measured with the profilometer and the diameter of the wear tracks. The wear factor was determined from a wear rate and a load using the following equation:

$$\text{Wear factor } (\text{mm}^3\,\text{N}^{-1}\text{m}^{-1}) = \frac{\text{Wear rate } (\text{mm}^3\,\text{m}^{-1})}{\text{Load (N)}} \quad (1)$$

The difference in two wear rates was tested by the F test [30].

The coatings and wear scar morphology were also observed with an optical stereo microscope (Nikon SMZ-2T) and the SEM.

3. Results and discussion

3.1. Diamond free metal carbide coating

In a previous paper [27], we reported that the carbide surface coating of Co–Cr–Mo implant alloys by a microwave plasma-assisted reaction was accompanied by codeposition of diamond film and soot covering a small area of the carbide surface. Furthermore, isolated diamond particles in a nest-like structure on the carbide surface were also found from previous wear tests and SEM observation. The problem of the formation of diamond film and soot or isolated diamond particles was overcome by controlling plasma process conditions.

The final processing conditions included replacing the graphite specimen holder, which had been conventionally used in plasma processing, with a tantalum wire basket. We also determined that rounding sharp edges of the specimen and polishing all the surfaces of each specimen before plasma processing were important in eliminating diamond crystal nucleation sites. Furthermore, proper specimen processing temperature was one of the critical conditions necessary to prevent diamond formation and therefore temperature fluctuation was minimized. The nest-like structures with diamond particles in previous studies could be detected as black dots under dark field observation of an optical stereo microscope (Fig. 1(a)). Therefore, every new coating was observed using the microscope dark field mode to confirm the absence of diamond particles. With these changes in plasma processing and use of surface inspections, 10-μm-thick metal carbide layers free of diamond film, soot, and diamond particles were produced on all surfaces of the Co–Cr–Mo alloy discs (Fig. 1(b)).

3.2. Surface morphology of ''brain coral-like'' carbide coatings

The silvery colored metal carbide coatings produced on Co–Cr–Mo discs in a 6-h processing time were about 10-μm-thick and consisted of a dense bottom layer and a top layer with the unique surface morphology shown in Figs. 2 and 3. In the top layer, lines or chains of peaks made up of linked crystalline grain clusters were randomly arranged and made up uniformly distributed convolutions similar to ''brain coral'' (Fig. 4).

The surface roughness parameters of these ''brain coral-like'' carbide layers by profilometry are given in Table I. The core roughness depth R_k and the reduced peak height R_{pk} which was nearly equal to the reduced valley depth R_{vk}, effectively quantified the surface characteristics of the carbide coatings. The value of $R_k + R_{pk} + R_{vk}$, 2.75 $\pm$ 0.55 μm, is slightly smaller than the PV_m. In addition to these roughness parameters

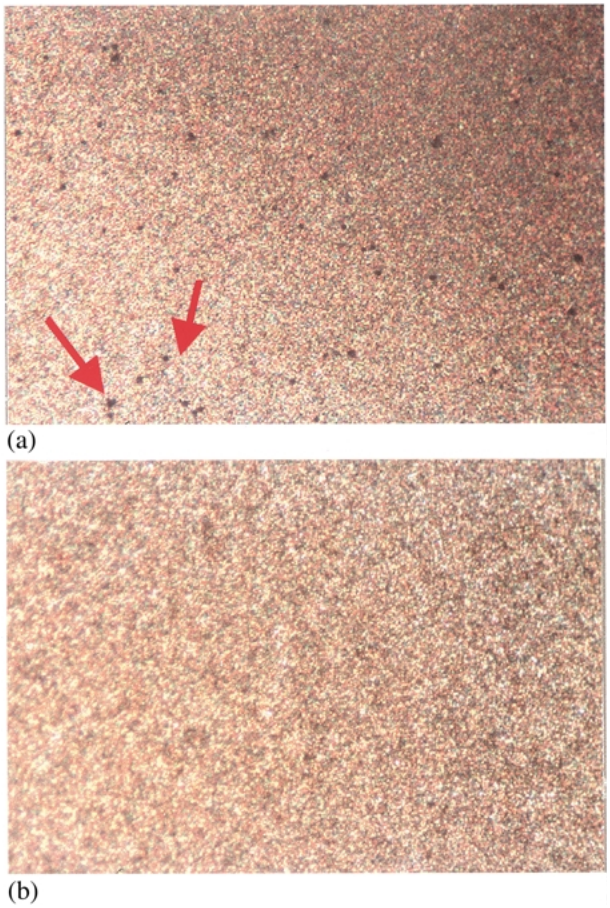

Figure 1 Carbide coated Co–Cr–Mo with black dots (a) and without black dots (b) under dark field observation with the × 60 magnification of an optical stereo microscope. The black dots indicate nest-like structures with diamond particles reported in a previous paper [27].

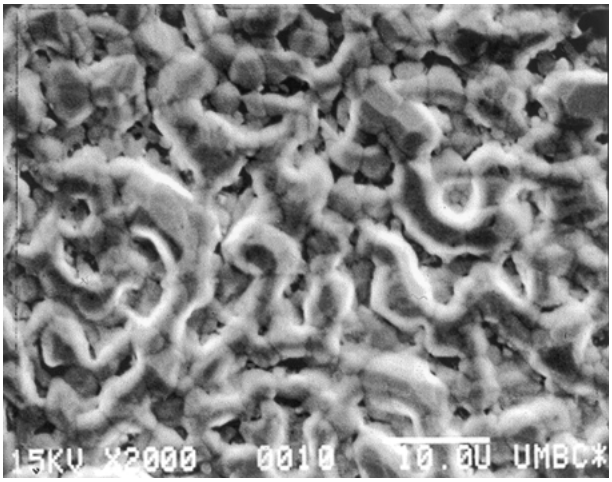

Figure 2 Scanning electron micrograph of a carbide coated Co–Cr–Mo disc.

commonly used in engineering fields, the average radius of summit curvature was estimated from surface profile plots to be 0.89 ± 0.71 μm. This value was required to calculate the ratio of the effective contact radius to the Hertz radius to be described in the next section.

The ''brain coral-like'' top layer of carbide coated Co–Cr–Mo discs may be simply and approximately described to consist of a 3-μm-thick peak-valley crystal cluster layer where the distance between chains of peaks

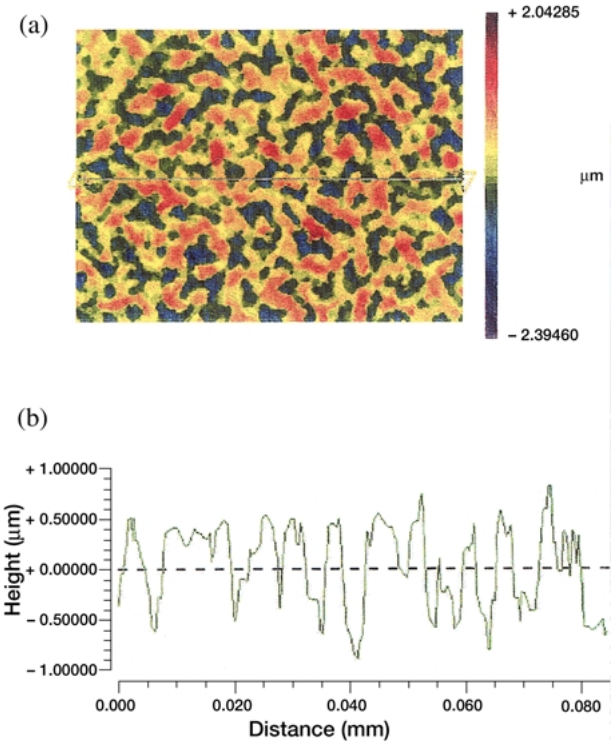

Figure 3 Profilometry surface map (a) and surface profile plot (b) of a carbide coated Co–Cr–Mo disc.

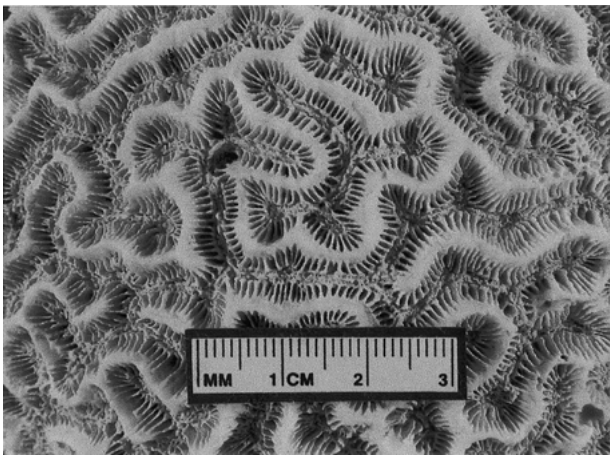

Figure 4 Picture of brain coral skeleton.

TABLE I Surface roughness parameters of carbide top layer by profilometry

Parameters	
Average roughness, R_a	0.53 ± 0.12 μm
Mean peak-to-valley height, PV_m	2.96 ± 0.59 μm
Core roughness, R_k	1.71 ± 0.37 μm
Reduced peak height, R_{pk}	0.56 ± 0.16 μm
Reduced valley depth, R_{vk}	0.48 ± 0.06 μm
Peak material ratio, M_{r1}	$7.23 \pm 2.20\%$
Valley material ratio, M_{r2}	$89.28 \pm 3.35\%$
Peak density	$21\,700 \pm 4780\,\text{mm}^{-2}$
Valley density	$20\,200 \pm 2940\,\text{mm}^{-2}$
Peak spacing	6.81 ± 0.72 μm
Valley spacing	7.00 ± 0.52 μm

(with average radius of summit curvature of $\sim 1\,\mu m$) or valleys is $\sim 7\,\mu m$ and the peak density (number of peaks per unit area) is almost equal to the valley density (number of valleys per unit area).

3.3. Wear tests

The profilometry surface profile oblique plots of wear scars (Fig. 5) demonstrate that the sapphire balls generated distinctive wear scars on uncoated and carbide coated Co–Cr–Mo discs. While the width and depth of the wear tracks on uncoated Co–Cr–Mo discs were uniform along the track circles ($\sim 1\%$ fluctuation in width and $\sim 4\%$ fluctuation in depth), those on carbide coated Co–Cr–Mo discs were more irregular along the track circles ($\sim 5\%$ fluctuation in width and $\sim 12\%$ fluctuation in depth). The rugged edges of wear tracks on carbide coated Co–Cr–Mo discs (Fig. 6) can be attributed to grain detachment and brittle fracture during the wearing process. The values of the wear track cross-sectional areas were obtained by averaging the values from eight locations separated by 45 degrees for uncoated discs, and by averaging the values from twelve locations separated by 30 degrees for carbide coated discs.

The linear regression analysis of the wear volume as a function of sliding distance is shown in Fig. 7 for the tests with no-lubrication at room temperature and the tests with deionized water lubrication at $37(\pm 2)\,^{\circ}C$. The correlation coefficient R^2 values for the least square linear fits were greater than 0.95 for all cases. The slope of the line represents the wear rate. Fig. 8 and Table II show the wear factors for each testing condition. The wear factor of uncoated Co–Cr–Mo discs with no-lubrication at room temperature is significantly greater

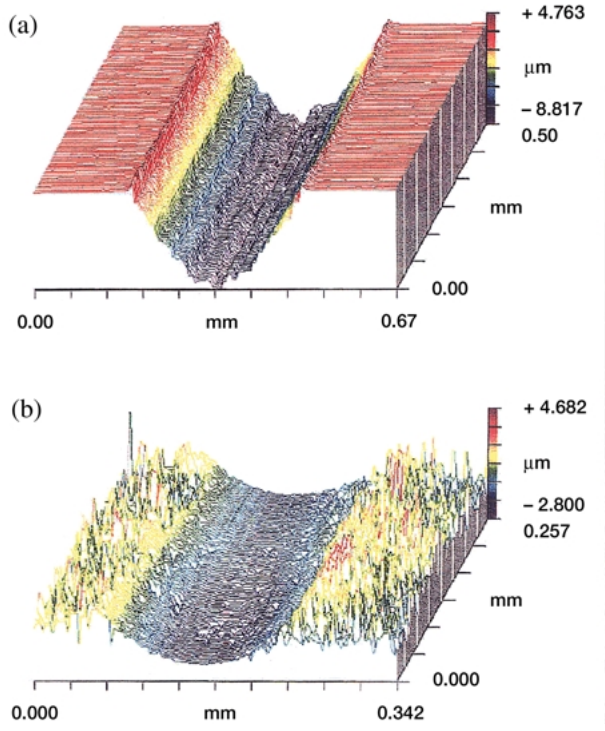

Figure 5 Profilometry oblique plots of wear scars on uncoated (a) and carbide coated (b) Co–Cr–Mo discs after 5-h wear tests with no-lubrication at room temperature.

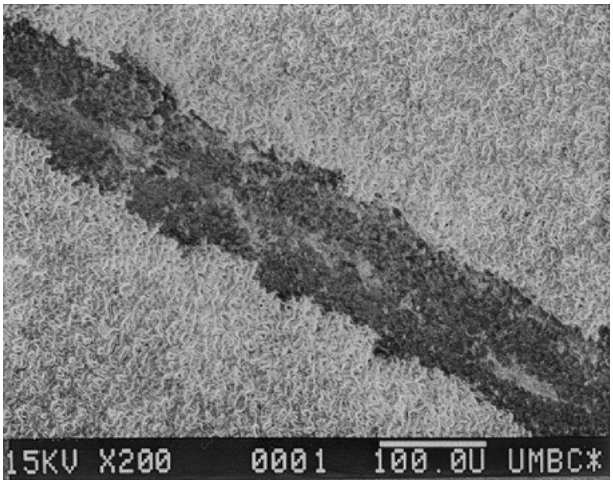

Figure 6 Scanning electron micrograph of a wear track on a carbide coated Co–Cr–Mo disc after 1 h of wear testing with no-lubrication.

than the wear factor of each other cases ($P < 0.005$). The effect of deionized water lubrication is clearly seen for uncoated Co–Cr–Mo discs and reduced the wear factor by one order of magnitude from that in the no-lubrication condition. Strongly adhered deposits were observed on

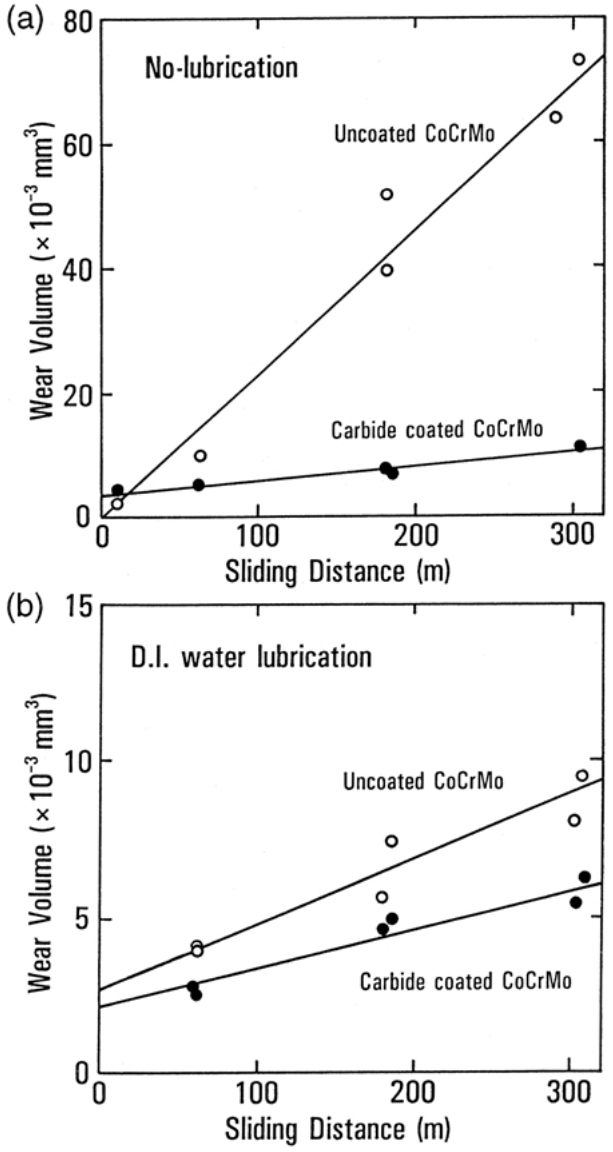

Figure 7 Graphs of the wear volume as a function of sliding distance for the test with no-lubrication at room temperature (a) and deionized water lubrication at $37(\pm 2)\,^{\circ}C$ (b).

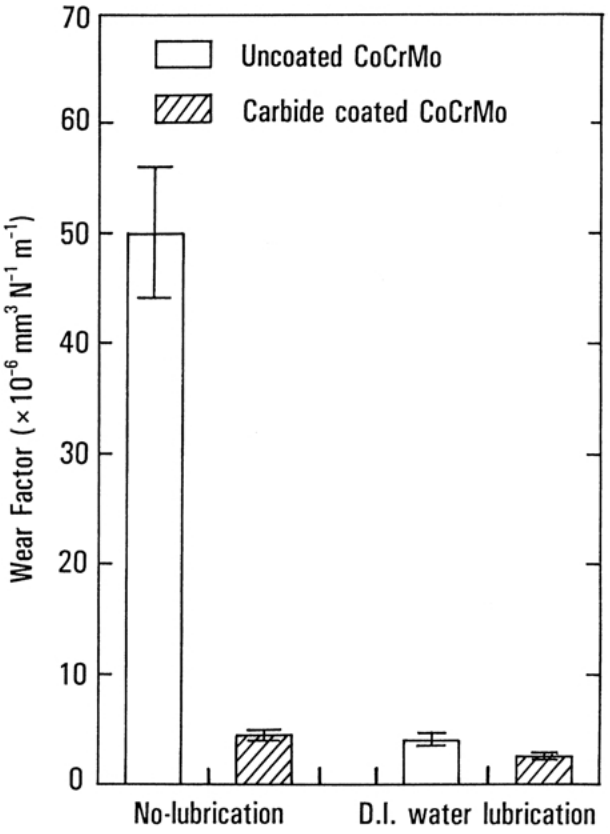

Figure 8 Wear factors for uncoated and carbide coated Co–Cr–Mo discs with no-lubrication and deionized water lubrication.

all the sapphire balls after no-lubrication wear tests of uncoated Co–Cr–Mo discs. The formation of alloy transfer material on the sapphire ball, indicating adhesive wear, was drastically reduced in the deionized water lubrication state. It is interesting to note that the wear factor of uncoated Co–Cr–Mo discs with deionized water lubrication obtained in this study, $4.2 \times 10^{-6}\,mm^3\,N^{-1}m^{-1}$, is very close to the wear factors of low carbon medical grade wrought cobalt chrome alloys reported recently [6] in spite of very different experimental conditions. Tipper *et al.* [6] reported wear factors of $\sim 4.5 \times 10^{-6}\,mm^3\,N^{-1}m^{-1}$ and $\sim 2.8 \times 10^{-6}\,mm^3\,N^{-1}m^{-1}$ for low carbon ($\sim 0.07\%$) alloy plates combined with a low carbon alloy pin and a high carbon alloy pin, respectively. They used a pin on plate reciprocator which applied a uniaxial frictional force and a nominal contact stress of 11.3 MPa, the test lubricant of 25% (v/v) newborn bovine calf serum supplemented by 0.1% sodium azide, and a reciprocating speed of 1 Hz with a stroke length of 30 mm. On the other hand, we used a ball on disc unidirectional rotational wear testing machine which applied an initial contact stress of 2.4 GPa estimated from the Hertzian theory of contact [31] between a low carbon ($\sim 0.05\%$) alloy disc and a sapphire ball, the test lubricant of deionized water, and a sliding speed of $17\,mm\,s^{-1}$. The good agreement between the two sets of data may be accidental but should be noted because the wear test conditions adopted in this study were not the standard described in the ASTM standard G 99-90 [32], nor conventional among wear simulation tests for artificial joint materials, but were harsh to accelerate the wear of carbide coated Co–Cr–Mo discs as the first step to study the wear behavior of this newly developed material. Since the wear factor of uncoated Co–Cr–Mo discs obtained here was not unrealistic, we maintained these conditions throughout this study.

TABLE II Wear factors for uncoated and carbide coated Co–Cr–Mo discs with no-lubrication and deionized water lubrication

	Wear Factor ($mm^3\,N^{-1}m^{-1}$)	
	No-lubrication	Deionized water lubrication
Uncoated Co–Cr–Mo	$(5.0 \pm 0.6) \times 10^{-5}$	$(4.2 \pm 0.6) \times 10^{-6}$
Carbide coated Co–Cr–Mo	$(4.5 \pm 0.5) \times 10^{-6}$	$(2.7 \pm 0.2) \times 10^{-6}$

The wear factor of carbide coated Co–Cr–Mo discs with no-lubrication, $4.5 \times 10^{-6}\,mm^3\,N^{-1}m^{-1}$, is converted to the dimensionless wear coefficient of $\sim 7 \times 10^{-5}$ by multiplying the wear factor by the hardness of carbide coated Co–Cr–Mo discs of HV ~ 1500 [27] ($= \sim 15$ GPa). This value of wear coefficient is in the range of mild to severe wear of nonmetal or ceramic materials [33, 34].

When a sapphire ball slides on the rough ''brain coral-like'' surface of a carbide coated Co–Cr–Mo disk, the sapphire ball encounters irregular and discrete carbide surface peaks. This situation bears some similarity to the case of the sliding counterfaces with a steep gradient in friction which causes stress concentration within the surface layer of the substrate. Joseph *et al.* [35] analyzed the model of a rigid indenter in frictional contact with an incompressible linear elastic half-space which represented a metallic orthopedic component in contact with a polymeric component. From the calculation of contact stresses in conditions of full slip and a pilot experimental study, they concluded that their model demonstrated that any type of surface inhomogeneity resulting in variable friction will lead to subsurface and surface stress concentrations and that these stress concentrations can initiate fatigue cracks which will propagate due to cyclic loading.

The stress concentrations caused by the surface morphology may have contributed to increasing the wear of carbide coated Co–Cr–Mo discs in this study. This effect may be more critical in the case of deionized water lubrication. The surface profile data of the worn scars showed that, in the case of the no-lubrication wear test, the wear particles were packed into the porous structure which originated from the ''brain coral-like'' morphology and produced a relatively smooth sliding contact surface. In contrast, the sliding contact surface in the case of deionized water lubrication maintained the rough structure relatively long because the flowing deionized water washed the wear particles away. The frictional effect of deionized water lubrication on the wear factor of carbide coated Co–Cr–Mo discs might have been partially compromised by the effect of stress concentrations.

The effect of wear particle packing also contributed to two other phenomena: the formation of microcracks on sapphire balls and the discrepancies between wear volume determined from surface profile cross-sectional area and wear volume calculated from the width of wear tracks.

Sapphire is a hard single crystalline aluminum oxide with hardness HV 2350 or 23 GPa [36] and was selected as a counterface material of this study to minimize the wear of the counterface. Most of the sapphire balls, after testing against carbide coated discs, showed damage, including micropits and microcracks near their top. Although each sapphire ball showed different degrees and areas of damage, which may be dependent on the crystal axis, the total damaged area of the six sapphire balls, in the case of deionized water lubrication, was about twice as large as that in the case of no-lubrication. It seems that the packed-in wear particles of carbide reduced the impact with the sapphire ball.

The discrepancies between the wear volume determined from the surface profile cross-sectional area and the wear volume calculated from the width of the wear tracks were clearly observed in the case of the carbide coated disc wear test with deionized water lubrication. Calculating wear volume from the width of wear tracks is one of the methods used to determine the wear volume described in the ASTM standard G 99-90 [32] and is based on the assumption that the wear track cross-section is a segment of a circle. The wear volumes obtained by two methods for the uncoated discs, with and without deionized water lubrication, and the carbide coated discs, without lubrication, agreed to within $\pm 10\%$. However, for carbide coated discs with deionized water lubrication, the wear volume determined from the surface profile cross-sectional area was always about 25% smaller than that calculated from the width of wear tracks. It has been known from the theory of contact mechanics that the effect of surface roughness is to reduce the maximum contact pressure and to spread the load over an area of radius greater than the Hertzian radius for smooth surfaces [37]. Since flowing deionized water washed the worn carbide particles away and refreshed the rough surface of the sliding contact area, the actual shape of the wear track cross-section was not a segment of a circle, but a flattened elliptical segment.

The ratio of the effective contact radius to the Hertz radius was estimated to be ~ 1.12 from the 25% wear volume difference. Greenwood and Tripp have developed a simplified theoretical model of the contact of a smooth sphere with a nominally flat rough surface [38]. In their model, contact occurs at a finite number of asperities whose summits are semispherical with equal radii and whose heights are distributed according to a Gaussian distribution. The iterative relation between forces and deformation of these asperities was used for computing self-consistent displacements and pressure distributions [38]. Using their numerical calculation results as a function of non-dimensional roughness parameters α and μ [37], and our profilometry data for the carbide coated Co–Cr–Mo discs, we obtained the ratio of the maximum contact pressure to the maximum Hertz pressure of ~ 0.65 and the ratio of the effective contact radius to the Hertz radius of ~ 1.29. The effect of the rough surface of the carbide layers may qualitatively explain the experimental result of wear volume difference. This phenomenon shows that the smoothing effect of the sliding contact area by the packed-in wear particles was reflected in the wear volume.

Despite their rough surface, which might have contributed to an increase in the wear factor, the wear factor of carbide coated Co–Cr–Mo discs was about 36% smaller than that of uncoated Co–Cr–Mo discs with deionized water lubrication ($P < 0.085$).

4. Conclusions

After the impurity problems in the carbide coatings on Co–Cr–Mo discs by the microwave plasma-assisted surface reaction were overcome, uncontaminated carbide coatings were produced. Wear tests were carried out using a ball-on-disk unidirectional configuration under harsh wear conditions. The wear factor of carbide coated Co–Cr–Mo discs was slightly smaller than that of uncoated Co–Cr–Mo discs with deionized water lubrication. To apply this newly developed carbide coated Co–Cr–Mo for use in artificial joints as a wear resistant material, the selection of the bearing material combination is important to effectively apply the high hardness and characteristic morphology of the carbide coatings. Additional wear testing using bovine serum lubrication with counterfaces of uncoated Co–Cr–Mo, Ti alloy, stainless steel, and/or polyethylene is necessary to determine wear characteristics for total joint replacement use. The next stage of this research is to control the surface morphology of carbide coatings on Co–Cr–Mo during and/or after plasma processing to obtain an optimized surface for artificial joints.

Acknowledgments

The authors would like to thank the Polymer Science Division of the National Institute of Standards and Technology for loaning them a wear test machine. This work was partially supported by a grant from the Arthritis Foundation.

References

1. H. C. AMSTUTZ, P. CAMPBELL, N. KOSSOVSKY and I. C. CLARKE, *Clin. Orthop. Relat. Res.* **276** (1992) 7–18.
2. M. JASTY, *J. Appl. Biomater.* **4** (1993) 273–276.
3. J. A. SCHEY, *Clin. Orthop. Relat. Res.* **329S** (1996) S115–S127.
4. H. MCKELLOP, S.-H. PARK, R. CHIESA, P. DOORN, B. LU, P. NORMAND, P. GRIGORIS and H. AMSTUTZ, *ibid.* **329S** (1996) S128–S140.
5. F. W. CHAN, J. D. BOBYN, J. B. MEDLEY, J. J. KRYGIER, S. YUE and M. TANZER, *ibid.* **333** (1996) 96–107.
6. J. L. TIPPER, P. J. FIRKINS, E. INGHAM, J. FISHER, M. H. STONE and R. FARRAR, *J. Mat. Sci: Mater. in Med.* **10** (1999) 353–362.
7. M. SEMLITSCH and H. G. WILLERT, *Proc. Instr. Mech. Engrs. Part H* **211** (1997) 73–88.
8. A. A. J. GOLDSMITH, D. DOWSON, G. H. ISAAC and J. G. LANCASTER, *ibid.* **214** (2000) 39–47.
9. D. DOWSON, C. M. MCNIE and A. A. J. GOLDSMITH, *Proc. Instr. Mech. Engrs. Part C* **214** (2000) 75–86.
10. M. L. SCOTT, J. I. PARTIN, A. W. EBERHARDT and J. E. LEMONS, in Trans. 25th Annual Meeting of Society for Biomaterials (1999) p. 136.
11. D. DOWSON, *Wear* **190** (1995) 171–183.
12. F. VILLERMAUX, L. BLAISE, B. CALÈS and J. M. DROUIN, in Trans. 25th Annual Meeting of Society for Biomaterials (1999) p. 135.
13. F. PRUDHOMMEAUX, E. CHAMPION, J. NEVELOS, A. MEUNIER, C. DOYLE and L. SEDEL, in *ibid.* p. 480.

14. P. J. FIRKINS, J. T. TIPPER, E. INGHAM, M. H. STONE, R. FARRAR and J. FISHER, in Trans. Sixth World Biomaterials Congress (2000) p. 55.
15. J. NEVELOS, E. INGHAM, C. DOYLE, A. NEVELOS and J. FISHER, in *ibid.* p. 875.
16. T. MURAKAMI, Y. SAWAE, S. DOI, S. TASHIMA and T. SHIMOTOSO, in *ibid.* p. 876.
17. F. VILLERMAUX, in *ibid.* p. 878.
18. P. FIRKINS, J. L. HAILEY and J. FISHER, *J. Mat. Sci.: Mater. in Med.* **9** (1998) 597–601.
19. T. L. JACOBS, J. H. SPENCE, S. S. WAGAL and H. J. OIEN, in ''Applications of Diamond Films and Related Materials: Third International Conference'', edited by A. Feldman, Y. Tzeng, W. A. Yarbrough, M. Yoshikawa and M. Murakawa (NIST, Gaithersburg, MD, 1995) pp. 753–756.
20. R. S. BUTTER and A. H. LETTINGTON, in *ibid.* 683–690.
21. V. C. JONES, D. C. BARTON, D. A. AUGER, C. HARDAKER, M. H. STONE and J. FISHER, in Trans. Sixth World Biomaterials Congress (2000) p. 1534.
22. S. AFFATATO, M. FRIGO and A. TONI, in *ibid.* p. 866.
23. H. MCKELLOP and T. V. RÖSTLUND, *J. Biomed. Mater. Res.* **24** (1990) 1413–1425.
24. A. CIGADA, S. FARE, F. BROSSA, L. PARACCHINI, M. ULIVI and J. C. BRIGNOLA, in Trans. Fifth World Biomaterials Congress (1996) p. 789.
25. P. SHIOSHANSI and D. E. FERGUSON, *Mat. Technol.* **8** (1993) 30–33.
26. J. P. HYVARINEN, K. SHINDHELM, W. R. WALSH, R. A. CLISSOLD, L. S. WIELUNSKI and M. V. SWAIN, in Trans. 25th Annual Meeting of Society for Biomaterials (1999) p. 133.
27. N. S. VANDAMME, L. QUE and L. D. T. TOPOLESKI, *J. Mat. Sci.* **34** (1999) 3525–3531.
28. L. MUMMERY, ''Surface Texture Analysis: The Handbook'' (Hommelwerke GmbH, West Germany, 1992) p. 23.
29. J. E. MCKINNEY, *Wear* **76** (1982) 337–347.
30. G. W. SNEDECOR and W. G. COCHRAN, ''Statistical Methods'' 7th ed. (The Iowa State University Press, Iowa, 1980) p. 385.
31. S. P. TIMOSHENKO and J. N. GOODIER, ''Theory of Elasticity'' 3rd ed. (McGraw-Hill, New York, 1970) p. 412.
32. ASTM designation G 99-90 in 1991 Annual Book of ASTM Standards, Vol. 03.02, Section 3 (ASTM, Philadelphia, PA, 1991) p. 387.
33. I. M. HUTCHINGS, ''Tribology: Friction and Wear of Engineering Materials'' (CRC Press, Boca Raton, FL, 1992) p. 200.
34. E. RABINOWICZ, ''Friction and Wear of Materials'' 2nd ed. (John Wiley & Sons, New York, 1995) p. 165.
35. P. F. JOSEPH, L. M. FLOOD, S. PULLELA-HO and M. LABERGE, in Trans. 25th Annual Meeting of Society for Biomaterials (1999) p. 130.
36. M. MOHANTY, R. W. SMITH, M. DE BONTE, J. P. CELIS and E. LUGSCHEIDER, *Wear* **198** (1996) 251–266.
37. K. L. JOHNSON, ''Contact Mechanics'' (Cambridge University Press, Cambridge, 1985) pp. 397–423.
38. J. A. GREENWOOD and J. H. TRIPP, *Trans. ASME, Series E, J. Appl. Mechanics* **34** (1967) 153–159.

Received 23 October 2001
and accepted 27 March 2002